

First joint Gravitational Waves search by the AURIGA-EXPLORER-NAUTILUS-Virgo collaboration

F. Acernese¹², P. Amico²⁰, M. Alshourbagy²¹, F. Antonucci²⁴,
S. Aoudia¹³, P. Astone²⁴, S. Avino¹², D. Babusci⁵, L. Baggio¹,
G. Ballardin², F. Barone¹², L. Barsotti²¹, M. Barsuglia¹⁸,
M. Bassan²⁶, Th. S. Bauer²⁵, M. Bignotto^{14,16}, S. Bigotta²¹,
S. Birindelli²¹, M.A. Bizouard¹⁸, C. Boccara¹⁹, M. Bonaldi^{29,30},
F. Bondu¹³, L. Bosi²⁰, C. Bradaschia²¹, S. Braccini²¹, J.F.J. van
den Brand²⁵, A. Brillet¹³, V. Brisson¹⁸, D. Buskulic¹,
G. Cagnoli⁴, E. Calloni¹², E. Campagna⁴, M. Camarda¹⁵, F.
Carbognani², P. Carelli^{10,26}, F. Cavalier¹⁸, R. Cavalieri²,
G. Cavallari⁶, F. Cavanna^{9,10}, G. Cella²¹, M. Cerdonio^{14,16},
E. Cesarini⁴, E. Chassande-Mottin¹³, A. Chincarini⁸,
A.-C. Clapson¹⁸, F. Cleva¹³, E. Coccia²⁶, L. Conti^{14,16}, C.
Corda²¹, A. Corsi²⁴, F. Cottone²⁰, J.-P. Coulon¹³, E. Cuoco², S.
D'Antonio²⁴, A. Dari²⁰, V. Dattilo², M. Davier¹⁸, M. del
Prete²¹, R. De Rosa¹², L. Di Fiore¹², A. Di Lieto²¹,
A. Di Virgilio²¹, M. Drago^{14,16}, F. Dubath⁷, B. Dujardin¹³, M.
Evans², V. Fafone¹³, P. Falferi^{29,30}, I. Ferrante²¹, F. Fidecaro²¹,
I. Fiori², R. Flaminio^{1,2}, S. Foffa⁷, P. Fortini³, J.-D. Fournier¹³,
S. Frasca²⁴, F. Frasconi²¹, L. Gammaitoni²⁰, F. Garufi¹²,
G Gemme², E. Genin², A. Gennai²¹, A. Giazotto^{2,21},
G. Giordano⁵, L. Giordano¹², V. Granata¹, C. Greverie¹³,
D. Grosjean¹, G. Guidi⁴, S. Hamdani², S. Hebri²,
H. Heitmann¹³, P. Hello¹⁸, D. Huet², S. Kreckelbergh¹⁸,
P. La Penna², M. Laval¹³, N. Leroy¹⁸, N. Letendre¹, N.
Liguori^{14,16}, S. Longo¹⁷, B. Lopez², M. Lorenzini⁴, V. Lorette¹⁹,
G. Losurdo⁴, J.-M. Mackowski¹¹, M. Maggiore⁷, E. Majorana²⁴,
A. Marini⁵, C. N. Man¹³, M. Mantovani²¹, F. Marchesoni²⁰,
F. Marion¹, J. Marque², F. Martelli⁴, A. Masserot¹, F.
Menzinger², R. Mezzena^{27,30}, Y. Minenkov⁹, L. Milano¹², A.
Mion^{27,30}, I. Modena²⁶, G. Modestino⁵, C. Moins², A. Moleti²⁶,
J. Moreau¹⁹, N. Morgado¹¹, S. Mosca¹², B. Mours¹,
G. P. Murtas⁵, I. Neri²⁰, F. Nocera², A. Ortolan¹⁷, G.
Pagliaroli²⁶, O. Palamara⁹, G.V. Pallottino²⁴, C. Palomba²⁴,

**F. Paoletti^{2,21}, S. Pardi¹², R. Parodi⁸, A. Pasqualetti²,
R. Passaquieti²¹, D. Passuello²¹, G. Piano Mortari^{9,10},
F. Piergiovanni⁴, L. Pinard¹¹, G. Pizzella²⁶, S. Poggi²⁸,
R. Poggiani²¹, G.A. Prodi^{27,30}, M. Punturo²⁰, P. Puppò²⁴, S. van
der Putten²⁵, L. Quintieri⁵, P. Rapagnani²⁴, V. Re^{27,30},
T. Regimbau¹³, A. Remillieux¹¹, F. Ricci²⁴, I. Ricciardi¹², A.
Rocchi²⁶, R. Romano¹², F. Ronga⁵, P. Ruggi², G. Russo¹², F.
Salemi^{27,30}, S. Solimeno¹², A. Spallicci¹³, R. Sturani⁷, L.
Taffarello¹⁶, M. Tarallo²¹, R. Terenzi²⁶, M. Tonelli²¹, A.
Toncelli²¹, G. Torrioli^{22,24}, E. Tournefier¹, F. Travasso²⁰, C.
Tremola²¹, R. Vaccarone⁸, G. Vajente²¹, G. Vandoni⁶, G.
Vedovato¹⁶, D. Verkindt¹, F. Vetrano⁴, A. Viceré⁴, A.
Vinante^{29,30}, J.-Y. Vinet¹³, M. Visco^{23,26}, S. Vitale^{27,30},
H. Vocca²⁰, M. Yvert¹, J.P. Zendri¹⁶**

¹Laboratoire d'Annecy-le-Vieux de physique des particules (LAPP), IN2P3/CNRS, Université de Savoie, BP 110, F-74941, Annecy-le-Vieux, CEDEX, France;

²European Gravitational Observatory (EGO), Via E. Amaldi, I-56021 Cascina (PI) Italy;

³ Dipartimento di Fisica, Università di Ferrara and INFN, Sezione di Ferrara, I-44100 Ferrara, Italy

⁴INFN - Sezione Firenze/Urbino Via G.Sansone 1, I-50019 Sesto Fiorentino; and/or Università di Firenze, Largo E.Fermi 2, I - 50125 Firenze and/or Università di Urbino, Via S.Chiera, 27 I-61029 Urbino, Italy;

⁵ INFN, Laboratori Nazionali di Frascati, Frascati, Italy

⁶ CERN, Geneva, Switzerland

⁷ Dep. de Phys. Théorique, Université de Genève, Genève, Switzerland

⁸ INFN, Sezione di Genova, Genova, Italy

⁹ INFN, Laboratori Nazionali del Gran Sasso, Assergi, L'Aquila, Italy

¹⁰ Università dell'Aquila, Italy

¹¹LMA 22, Boulevard Niels Bohr 69622 - Villeurbanne- Lyon Cedex France;

¹²INFN - Sezione di Napoli and/or Università di Napoli "Federico II" Complesso Universitario di Monte S. Angelo Via Cintia, I-80126 Napoli, Italy and/or Università di Salerno Via Ponte Don Melillo, I-84084 Fisciano (Salerno), Italy;

¹³Department Artemis - Observatoire de la Côte d'Azur, BP 42209, 06304 Nice Cedex 4, France;

¹⁴ Dipartimento di Fisica, Università di Padova, Via Marzolo 8, 35131 Padova, Italy

¹⁵ Dipartimento di Ingegneria Informatica, Università di Padova, Via G. Gradenigo 6a, 35131 Padova, Italy

¹⁶ INFN, Sezione di Padova, Via Marzolo 8, 35131 Padova, Italy

¹⁷ INFN, Laboratori Nazionali di Legnaro, 35020 Legnaro, Padova, Italy

¹⁸LAL, Univ Paris-Sud, IN2P3/CNRS, Orsay, France;

¹⁹ESPCI - 10, rue Vauquelin, 75005 Paris - France;

²⁰INFN Sezione di Perugia and/or Università di Perugia, Via A. Pascoli, I-06123 Perugia - Italy;

²¹INFN - Sezione di Pisa and/or Università di Pisa, Via Filippo Buonarroti, 2 I-56127 PISA - Italy;

²² CNR, Istituto di Fotonica e Nanotecnologie, Roma, Italy

²³ INAF, Istituto Fisica Spazio Interplanetario, Roma, Italy

²⁴INFN, Sezione di Roma and/or Università "La Sapienza", P.le A. Moro 2, I-00185, Roma, Italy;

²⁵National Institute for Nuclear Physics and High Energy Physics, NL-1009 DB Amsterdam and/or Vrije Universiteit, NL-1081 HV Amsterdam, The Netherlands.

²⁶ INFN, Sezione di Roma Tor Vergata and/or Università di Roma Tor Vergata, Via della Ricerca Scientifica, 1 00133 Roma, Italy

²⁷ Dipartimento di Fisica, Università di Trento, I-38050 Povo, Trento, Italy

²⁸ Consorzio Criospazio Ricerche, I-38050 Povo, Trento, Italy

²⁹ Istituto di Fotonica e Nanotecnologie, CNR-Istituto Trentino di Cultura, I-38050 Povo (Trento), Italy

³⁰ INFN, Gruppo Collegato di Trento, Sezione di Padova, I-38050 Povo, Trento, Italy

E-mail: Lucio.Baggio@lnl.infn.it, guidi@uniurb.it, virginia.re@lnl.infn.it

Abstract. We present results of the search for coincident burst excitations over a 24 hours long data set collected by AURIGA, EXPLORER, NAUTILUS and Virgo detectors during September 2005. The search of candidate triggers was performed independently on each of the data sets from single detectors. We looked for two-fold time coincidences between these candidates using an algorithm optimized for a given population of sources and we calculated the efficiency of detection through injections of templated signal waveforms into the streams of data. To this purpose we have considered the case of signals shaped as damped sinusoids coming from the galactic center direction. In this framework our method targets an optimal balance between high efficiency and low false alarm rate, aiming at setting confidence intervals as stringent as possible in terms of the rate of the selected source models.

1. Introduction

The network composed by the three gravitational wave (GW) resonant detectors AURIGA[1, 2], EXPLORER and NAUTILUS [3, 4] and the interferometer Virgo[5] (hereafter called Virgo-bars network) is heterogeneous, as its single components differ for spectral sensitivity (see figure 1) and antenna pattern.

In the past years, various searches for GW signals have been independently performed by individual detectors or by networks of resonant bars (IGEC, [6, 7], ROG [8]) or interferometers [9, 10, 11]. In the latter cases the networks were homogeneous: almost same antenna pattern (neglecting a small misalignment), similar (within a factor 2) integrated sensitivity and roughly same observed frequency range (or detection bands). Therefore, a GW burst would produce approximately the same response in all the detectors of the network (notably, irrespective of direction and polarization of the source). In such cases the magnitude of observed signals can be compared directly.

Previous burst searches among detectors with different spectral sensitivity and orientation were performed by the TAMA and LIGO Scientific Collaboration [12] among interferometers and by the AURIGA and LIGO Scientific Collaborations [13, 14] between interferometers and a resonant bar.

The proposed network search strategy for the Virgo-bars data analysis takes as a starting point the IGEC coincidence search for burst GW events. This search was innovative with respect to previous searches as it preserved the detection efficiency by selecting the detectors which, time to time, had comparable directional sensitivity for sources located at a given sky position. In that case, however, there was no optimization on detection efficiency and the analysis relied on identical antenna patterns for the detectors. Instead, for the Virgo-bars network, it is necessary to further develop the idea included in the IGEC strategy. The detection efficiency will be determined by studying the software injections (Mock Data Challenge, in the following referred to as MDC) of a given collection of target waveforms. The approach attempted in this work is to use the efficiency computation both to tune the analysis parameters and to calibrate the final results, a step missing in ref. [7].

The results we present here are obtained in the simpler case of fixed time coincidence windows and two-fold coincidences among different detectors pairs. The coincident counts, divided by the detection efficiency and by the observation time, become then observed rates (or upper limits on rates) for that particular source population. The relevance of this study is methodological due to the short observation time, the uncertainty on the detectors calibrations and to some approximations in the production of the MDC.

The paper is organized as follows: in section 2 we introduce the target GW signals and the source population we are dealing with. An overview of the exchanged data is presented in section 3. Section 4 presents the results obtained from software injections of GW signals into the data and the related estimates of the single detectors detection efficiencies and time errors. The coincident search strategy adopted in this work as

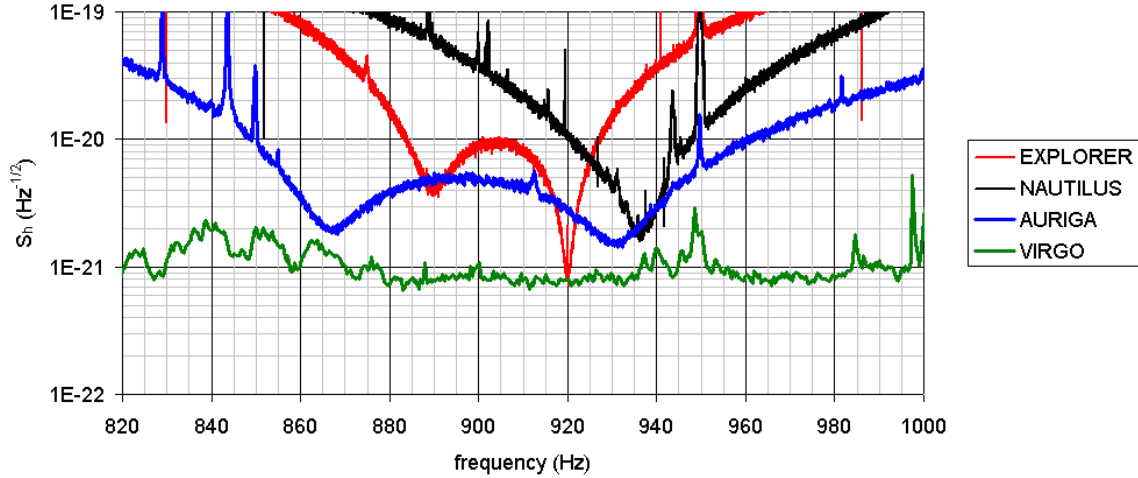


Figure 1. Typical spectral density of calibrated noise for the three resonant bar detectors during 2005 and for the Virgo interferometer in Sept 2005.

well as the background estimation method and confidence of detection are described in section 5. The results and final remarks are presented in section 6 and 7 respectively. Finally, we report in Appendix A a summary of the pipeline main steps and in Appendix B a complete calculation of the energy budget associated to the injected signals.

2. Target signals

The class of transient GW signals is extremely large; moreover, such signals may be generated by a large variety of astrophysical sources. In this scenario, we have chosen to constrain the source population to the ensemble of waveforms that can be analytically described as a damped sinusoid (DS) with central frequency ranging within the bars bandwidths (850-950 Hz) and characterized by decaying times spanning at most a few tens of milliseconds. This choice is due to the different spectral densities of the various detectors in the collaboration (see figure 1), so that the interesting signals for our specific network are the ones whose power is concentrated in the bars most sensitive frequency range.

A typical damped sinusoid (DS) waveform is described by the following template:

$$u(t) \propto e^{-t/\tau} \cos(2\pi f_0 t + \varphi_0) \quad (1)$$

where f_0 is the central frequency and τ the damping time. These signals can be produced for instance by a ring-down phase following the merger of two black holes [15]. Other sources whose emission can be modelled by (1) are f-modes from neutron stars. The f-modes could produce a wave with variable frequency and damping time, which may sweep inside the observed frequency band [16]. To make a realistic detection, the energy release should be about $10^{-3} - 10^{-4} M_\odot$ for a galactic event (see Appendix B.1).

The astrophysical model for our source population considers elliptically polarized signals (as sources angular momenta should have random directions with respect to the

line of sight to the earth) incoming from the Galactic Center.

3. Overview of exchanged data

The exchanged data consists of event lists corresponding to 24 hours of data taking, starting from GPS time 810774700, or UTC time 14 Sep 2005 23:11:27. This choice corresponds to the longest stretches of continuous acquisition during the so called “C7” run of Virgo, when AURIGA, EXPLORER and NAUTILUS were in stable operation.

Each group exchanged the triggers found above a chosen threshold by their respective burst event search algorithms. No further tuning of parameters and amplitudes has been done at this stage: a cut based on the magnitude of the events can be optimally set up afterwards based on the relative performances of the detectors at any given time. This selection reduces the number of background events without severely affecting the efficiency for a specific injection class.

Before exchanging all the data, the time information has been offset by a secret time shift within each group. This was done in order to prevent any bias which might arise by looking at the zero-delay coincidence counts in the tuning phase of the analysis.

It has to be noticed that the amplitudes may suffer from a systematic error due to the calibration uncertainty of each detector. This error is declared to be at most $\sim 30\%$ for Virgo, $\sim 20\%$ for EXPLORER and NAUTILUS, and $\sim 10\%$ for AURIGA.

3.1. Event Trigger Generators

From the Virgo side, Power Filter[17] was the chosen Event Trigger Generator. Power Filter searches on whitened data for a power excess using different time analysis windows and different frequency bands and it uses as an indicator of the signal magnitude the (logarithmic) Signal to Noise Ratio (SNR). Events were exchanged at (logarithmic) $SNR \geq 3.4$.

AURIGA group has successfully tested on its data an implementation of WaveBurst Event Trigger Generator, which is an excess power algorithm based on the wavelet transform developed by the LIGO Scientific Collaboration [18]; the exchange threshold was set at amplitude $SNR \geq 4.5$. For the NAUTILUS and EXPLORER detectors the Event Trigger Generator is an adaptive linear filter matched to the impulse response [19, 20]. The amplitude calibrated for the impulse response and the SNR were exchanged for each event and the exchange threshold was fixed at $SNR \geq 3.8$.

3.2. Data quality: the correlograms

The histogram of time difference among the outputs of the local Event Trigger Generators (or *correlogram*) with a given bin size is equivalent to counting coincidences with fixed window as a function of the time delay. The absence of cross-correlation is a useful hint that the coincidences at some delay may be considered as representative of the accidental coincidence probability at zero delay.

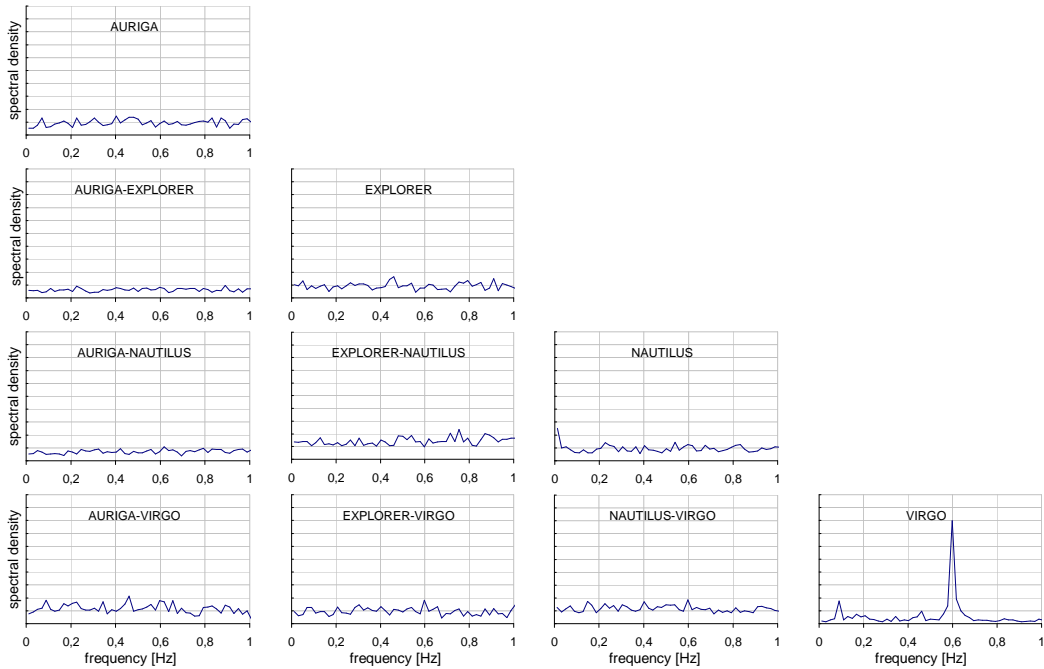


Figure 2. Spectral densities of correlograms and cross-correlograms for AURIGA, EXPLORER, NAUTILUS and Virgo. The spectra are flat within errors for all cases but for Virgo, where a 0.6Hz noise line is dominant (this is visible as periodic ripples in the Virgo auto-correlogram)

While single detectors, like Virgo, show some level of auto-correlation in the correlogram of the background events, on the other hand the cross-correlogram is flat as expected for random Poisson point processes.

We found no evidence of modulation in the cross-correlation histogram up to ± 400 s. Looking at the histograms in the Fourier domain (see figure 2), the spectral density is flat for all detectors and detector couples, with the exception of Virgo, which presents a known strong peak at 0.6 Hz; this is the fundamental pendulum mode of the Virgo mirror suspension, whose excitation is only partially suppressed by the interferometer control loops.

4. Results from software injections

The injected GW signals consist of time series of sampled DS with f_0 within the sensitive frequency region for the resonant detectors, τ spanning between 1 and 30 ms (see table 1) and random elliptical polarization.

The source location is chosen at the Galactic Center. For each detector, a specialized time series is produced including the time delays and the amplitude attenuation due to antenna pattern (see for example the amplitude modulation on figure 6), using the SIESTA simulation software [21]. The simulated signals arrive at the Earth center approximately evenly spaced by 10 s (with a random jitter of ± 0.5 s),

producing a set of 8640 injections over the 24 hrs observation time.

In the following, when referring to the “amplitude” of the population, we mean the absolute h_{rss} amplitude of the wave, i.e. the amplitude at the earth of the unprojected wave tensor (see Appendix B.1). The generated waveform amplitudes for the coincidence analysis range between $h_{rss} = 10^{-20} \text{ Hz}^{-1/2}$ and $10^{-18} \text{ Hz}^{-1/2}$ in order to span the curve of efficiency vs h_{rss} for all the detectors – see section 4.3.

We acknowledge a coarse approximation in the algorithm that calculates the samples amplitudes for the MDC, resulting in an overall underestimation of the injected signal strength h_{rss} with respect to the declared value. The effect of such approximation is fully negligible for the most energetic signals, while it may cause a spurious loss of efficiency at the lowest amplitudes and for the less sensitive detectors. Nevertheless, the reported results are conservative and the methodological relevance of this work is not affected.

4.1. Time errors

The timing error of all search algorithms is heavily dominated by systematic biases. This is typical of algorithms that are not matched to the particular signal one is looking for. For instance, for the Virgo detector, the Power Filter filter bandwidth is $\sim 100 \text{ Hz}$ in the narrowest channel, and the time of arrival is determined by the time when the signal reaches its maximum amplitude. Because of this the biases for 1 ms and 10 ms long DS are 0.8 ms and 3.6 ms respectively.

For the AURIGA detector, the bandwidth is narrower, causing a larger distortion of the signal. Moreover the time associated to the event is computed as the baricenter of the signal profile above threshold. The amount of the bias depends strongly on the time duration and also on the central frequency of the signal. Altogether, for the durations $\leq 30 \text{ ms}$ the bias for DS ranges from $\sim 3 \text{ ms}$ to $\sim 30 \text{ ms}$ depending on the central frequency [22].

The linear filter matched to a delta signal is unbiased for wide band signals, such as 1 ms long DS, but it is more biased as the signal duration gets longer [23]. For the considered DS the worst time error of EXPLORER and NAUTILUS was of the order of 8 ms and 16 ms for damping time $\tau = 10 \text{ ms}$ and $\tau = 30 \text{ ms}$ respectively.

Table 1. The parameter space of DS signals is described by their central frequency f_0 and their decay time τ . The latter takes values spaced logarithmically by about a factor 3, while the frequency axis is sampled at a special subset of frequencies, which was chosen on the basis of the typical narrow-band power spectral densities of the bars.

τ (ms)	f_0 (Hz)
1	914
3	882 946
10	866 898 930
30	866 874 906 930 938

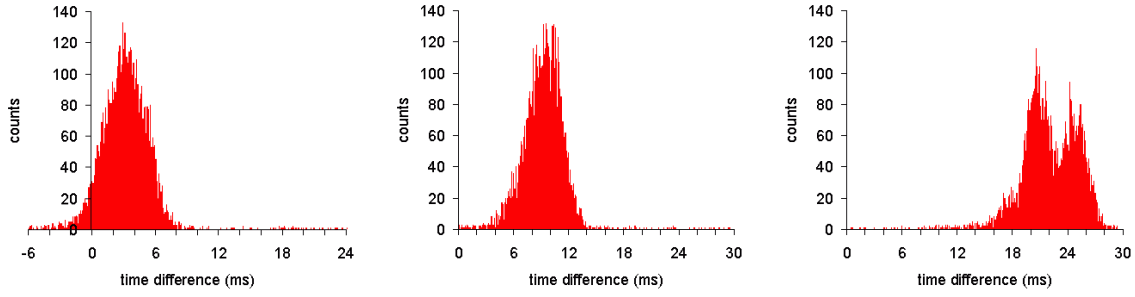


Figure 3. Distribution of time differences of detected events in coincident injection of DS(914Hz;1ms) (*left*), DS(930Hz;10ms) (*center*) and DS(930Hz;30ms) (*right*), at $h_{rss} = 10^{-18} \text{ Hz}^{-1/2}$ for the couple AURIGA-Virgo.

In figure 3 we see for example that the maximum time difference between AURIGA and Virgo is ≤ 30 ms.

4.2. Distribution of amplitudes of accidental events and injected signals

The single detector search algorithms provide different estimates of the magnitude of the signal. Although not directly comparable among different detectors, the event magnitudes provided by each detector show how much the population of injected waveforms stems from the noise distribution. An example can be seen in figure 4.

4.3. Efficiency of detection

The software injections have been used also to monitor the detection efficiency of the single detectors. The efficiency is computed for different waveform amplitudes and using a ± 40 ms time window around the injection times: we look for coincidences between the injected signals and the events found by the Event Trigger Generators. The calculation of the efficiency is based on the nominal 24 hours allocated for this search. Consequently, dead times in the data due, for example, to epoch vetoes affect the average efficiency. This is the case for detector Virgo: its duty time is, in fact, far less than 100% in the 24 hours considered (about 7 hours are vetoed out because of bad data quality), which finally reduces the attainable average efficiency (see figure 5). The resonant detectors have instead a very stable duty cycle and they show improved performances with respect to Virgo when the signal is fully contained in their bandwidth (which requires special selection of central frequency and long signal duration).

In conclusion, our definition of efficiency includes also dead times when data are missing or vetoed out from the nominal set, as we are interested in whether or not the network was able to recover the injected signals. We will comply with this comprehensive definition of efficiency throughout the paper.

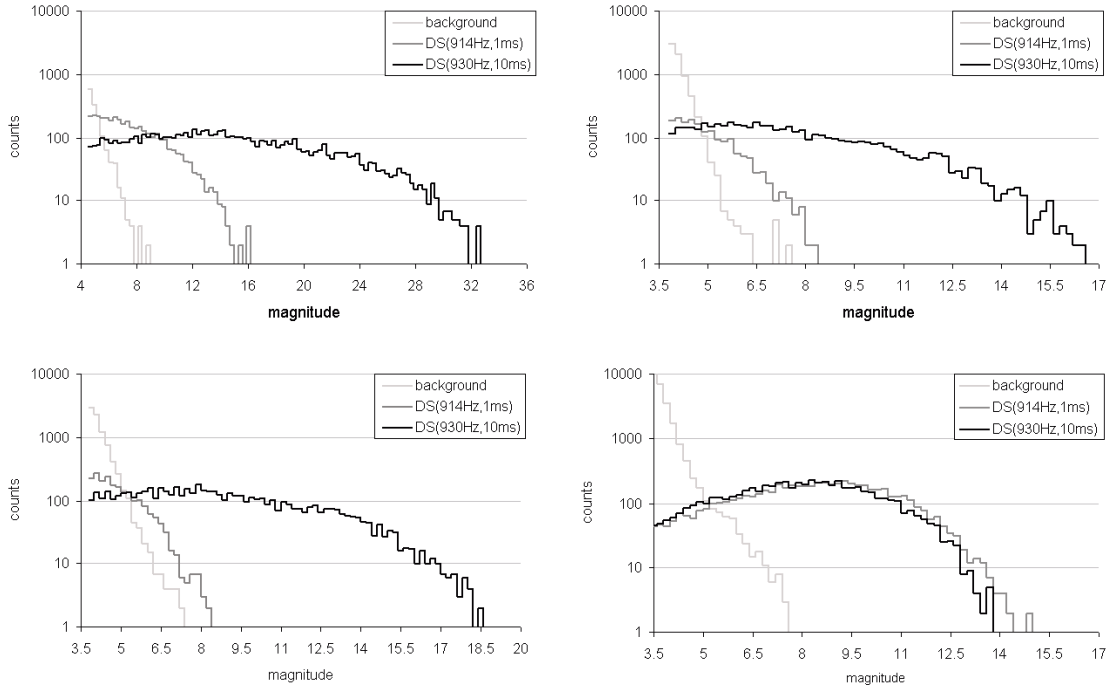


Figure 4. Distribution of detected “event magnitudes” for background events and injections of DS(914Hz;1ms) and DS(930Hz;10ms) at $h_{rss} = 10^{-19} Hz^{-1/2}$ for AURIGA (*top-left*), EXPLORER (*top-right*), NAUTILUS (*bottom-left*) and Virgo (*bottom-right*). The “magnitude” can be the SNR ratio given by WaveBurst algorithm (AU), the one given by a linear matched filter (EX and NA) and the logarithmic SNR of Power Filter (Virgo). Given the very different meaning of these quantities, the plots obtained for different detectors cannot be compared directly.

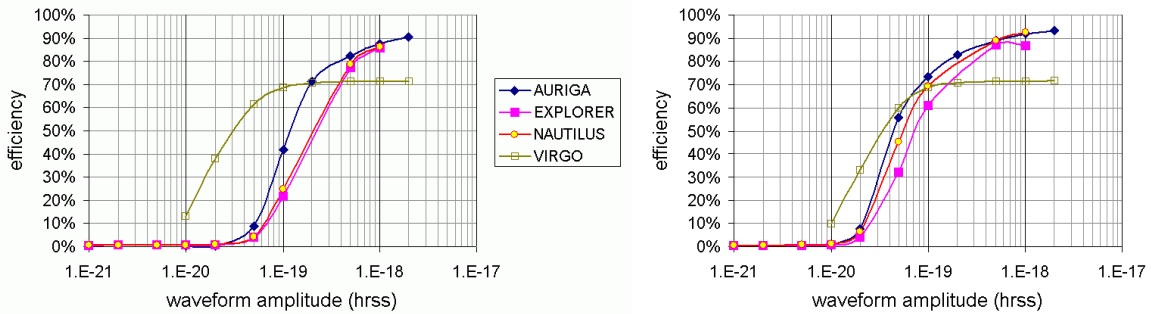


Figure 5. Efficiency of detection for the four detectors when recovering injections of DS(914Hz;1ms) (*left*) and DS(930Hz;10ms) (*right*) at different values of h_{rss} . In the selected 24 hours, ~ 7 hours of Virgo data have been excluded by epoch vetoes based on data quality. That is why efficiency levels at about 70%.

5. Coincidence analysis

A coincidence between two detectors is defined as the fulfilling of the relation

$$\left| t_{j_k}^{(k)} - t_{j_h}^{(h)} - \Delta t_{hk} \right| < T_w \quad (2)$$

where $t_{j_k}^{(k)}$ is the estimated time of arrival of the j_k signal in the detector labelled k and Δt_{hk} is the time of flight between the sites of the two detectors. For the case of our network and for signals coming from the Galactic Center, the maximum time delay ranges between 0.3 ms for the couple Virgo-AURIGA and 2.4 ms for EXPLORER-NAUTILUS. From the results of the MDC injections (specifically, sec.4.1), we set in the following $T_w = 40$ ms. After the tuning of the analysis (which will be described in the following sections), we checked, for all the configurations shown on table 2, that the loss in the overall efficiency with this coincidence time window is at most 1%.

5.1. Thresholds optimization

As we can see from figure 4, for a small increase in the magnitude threshold a large reduction of the background counts can be expected. The accidental coincidence rate between two detectors is proportional to the event rate of the two detectors, so we can act on one of the two thresholds, or on both. The trade off is the reduction of detection efficiency. Sometimes the detected magnitude of the injected events is large enough to increase the threshold up to exclude any background coincidence, while in other time periods lower thresholds are preferred to preserve the detection efficiency.

In order to quantify these statements, we consider a gain function defined as the ratio between the average efficiency and the square root of the background counts. The rationale for this choice derives from the procedure to set confidence intervals on the number of true coincidences. In fact, the background of accidental coincidences can always be subtracted from the found (total) number of coincidences. The residual of the subtraction is –loosely speaking– the number of truly correlated events between the detectors. In this sense, our gain function is the ratio between the average efficiency and the fluctuations of the background. As our source population is set in the Galactic Center, we apply a time varying threshold (calculated every 30 minutes by maximizing the gain function, as above stated). This implies that for each time bin the threshold is set at the level corresponding to the maximum of the gain function for the pair of detectors. The overall result is that we apply over the entire data set and for each detector of the couple a non-constant cut on the event magnitude, using a threshold set every 30 minutes (the analysis pipeline is discussed in more detail in Appendix A).

Figure 6 shows an example of such adaptive thresholds. As Virgo, in this example, can see the injected events much better than AURIGA, the algorithm starts with raising Virgo threshold. This cleans up most of the coincident events. The efficiency of AURIGA is therefore preserved, as its threshold is left almost untouched.

5.2. Background and efficiency of the network

The efficiency of detection is empirically defined by the sets of data containing MDC injections. The ratio between the coincident events due to injections found in the detector couple under study and the known number of injected events gives the empirical estimate of the efficiency ‡.

For the background estimation, we first take care of the (possible) true correlated events present in the data by shifting the times of the event lists of different detectors before looking for coincidences in time. By repeating this operation a number of times, we get renewed instances of the counting experiment: we will refer to this procedure as *time delay analysis*. Altogether, the coincidences from hundreds of shifted configurations provide a rich population from which we can determine the main parameters of the background distribution. If the time slide measurements are independent from each other, the number of accidental coincidences in each time shift should be Poisson distributed. We tested this hypothesis by means of a χ^2 test just on those searches which have an high expected number of accidental coincidences, N_b , so to ensure a sufficiently large data sample. The corresponding p-values were not inconsistent with the Poisson model for the expected number of accidentals.

The optimization procedure described in the previous section determines the cuts on the data set based on a function of the estimated background and efficiency. Hence these two estimates will be biased, sometimes severely, and cannot be used for setting confidence intervals. For this reason, we preliminarily divide the original data (accidental coincidences and MDC injections) into two equal size subsets: one is used in the optimization phase. The threshold levels obtained at the end of the optimisation are subsequently applied to the second halves of the data, without further tuning. Background counts and efficiency are thus computed from this second subset, giving unbiased estimates.

5.3. Setting confidence intervals

We first set the confidence interval on the number of correlated events detected in coincidence, following a unified approach in the spirit of [24]. However, the procedure we adopt to build the confidence belt is different and its fundamentals has been discussed in [7] and [25]. We start by considering the likelihood of the number of coincidences at zero-delay N_c as a function of the expected values of the accidental counts and of the correlated events, N_b and N_{GW} respectively:

$$l(N_c; N_b, N_{GW}) = \frac{(N_b + N_{GW})^{N_c}}{N_c!} e^{-(N_b + N_{GW})} \quad (3)$$

The confidence intervals on N_{GW} are built by integrating the likelihood

$$I = \frac{\left[\int_{N_{inf}}^{N_{sup}} l(N_c; N_b, N_{GW}) dN_{GW} \right]}{\int_0^{\infty} l(N_c; N_b, N_{GW}) dN_{GW}} \quad (4)$$

‡ The contamination due to accidental coincidences was found to be negligible.

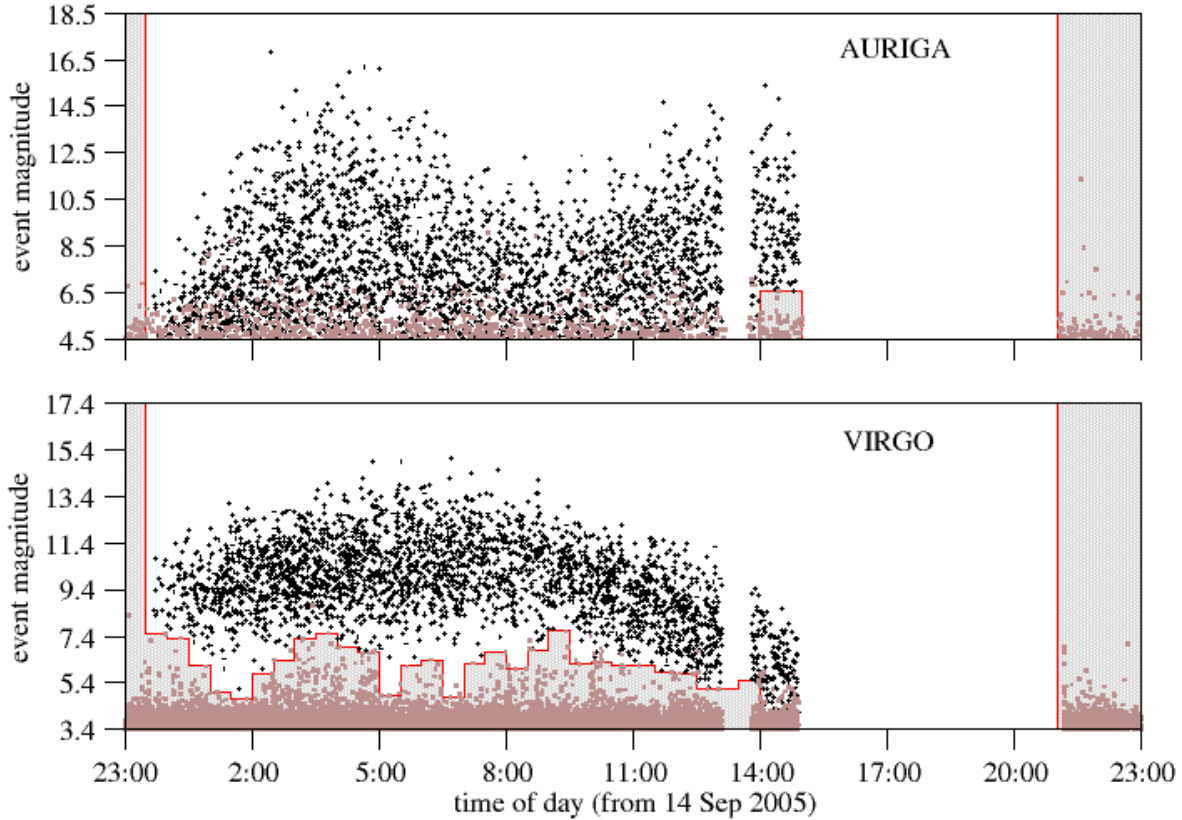


Figure 6. Example of threshold placing for detection optimization for the template DS(914Hz;1ms) at $h_{rss} = 10^{-19} \text{ Hz}^{-1/2}$ for the couple AURIGA (*above*) and Virgo (*below*). The abscissa represents the period of the exchanged 24 hours of data taking, the ordinate is the event magnitude given respectively by the WaveBurst and the PowerFilter algorithms. The light markers indicate background coincident events, the darker ones are events generated by injections. The modulation of the event magnitude by the antenna pattern is clearly visible in the two plots. The events form coincident couples, i.e. to each event in AURIGA the corresponding event in Virgo is plotted. Excluding one event from one detector automatically excludes the paired one in the other. Thus, given the relatively good separation of MDC events from background events in Virgo, the threshold here is raised up to the limit where basically all background events are excluded, while the threshold in AURIGA is left almost at its initial value.

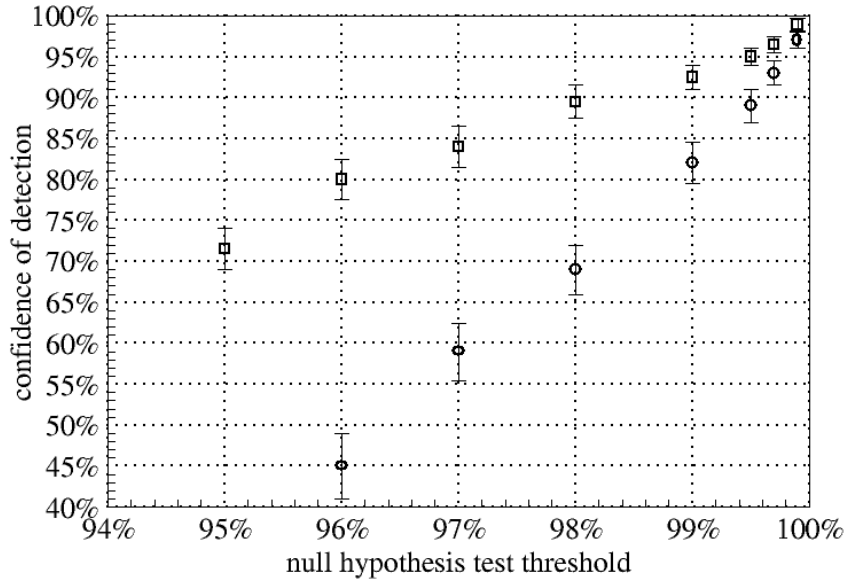


Figure 7. Measured global confidence of detection over all configurations *vs* nominal confidence of the null hypothesis test for each single search. The circles refer to the whole list of trials, the squares to the configurations which gave the best upper limits.

to find the smallest interval $[N_{inf}, N_{sup}]$ corresponding to the chosen I value. The set of these intervals computed for the possible N_c values makes the wanted confidence belt of N_{GW} vs N_c for fixed level of background N_b . It is well known that the I cannot be interpreted as a frequentist probability; therefore, the actual probability that the confidence intervals $[N_{inf}, N_{sup}]$ include the true N_{GW} value, i.e. the coverage, must be empirically determined by a Monte Carlo [25]. The quoted coverage is the minimum coverage ensured by the belt §.

In the present work, we modify the above procedure by adding a more stringent test of the null hypothesis in order to increase the coverage when $N_{GW} = 0$. In practice, we want a more stringent false alarm to issue a two-sided confidence interval with lower extreme greater than zero. This is done by performing a Poisson one-tail test on the found coincidences N_c assuming the null hypothesis, $N_{GW} = 0$. The significance of the test is set at a higher level than the coverage of the belt, as discussed in the next section. In case the test is passed, the lower extreme of the confidence interval N_{inf} is extended to zero.

§ Notice that at 95% coverage, the upper limit set by this belt is 3.6 counts when $N_c = 0$, regardless of the value of the background, N_b .

5.4. Multiple trials and global confidence

In this analysis we perform many searches for different signal waveforms and amplitudes by different detector pairs. The trial factor is therefore large and we are interested in controlling the global probability of false claim of the whole experiment. To estimate it, we considered the 400 different time-delayed configurations obtained by time shifting the original data set, assuming they are independent realizations of the experiment with no correlated events. The resulting coincidences has to be accidental and we can empirically estimate the distribution of these coincidence counts. We can then determine the global confidence of detection of the entire experiment as a function of the chosen significance of the null hypothesis test on each single trial. The results are shown as circle data points in figure 7. In particular, to have a global confidence of detection of at least 95%, we need to set the significance up to ~ 0.999 on the null hypothesis test for each single trial.

There is a trade off between the global false claim probability and the detection efficiency of the experiment: to decrease the false claim probability it becomes more difficult to recognize a true signal. For instance, with $N_b \sim 0.1$, as observed in most of the configurations, and the threshold of the 1-tail Poisson test set at 99.9%, we need at least 3 coincidences detected in a couple of detectors in order to reject the null hypothesis and make a claim for correlated events.

In order to reduce this drawback, we attempted to limit as much as possible the trial factor of the experiment. In particular, for each signal waveform and amplitude we considered only the results produced by the pair of detectors which was performing best (square data points in figure 7). To select the best performing pair, we compute fake upper limits per each pair under the assumption that the number of found coincidences is compatible to the expected background of the pair. Only the pair producing the more stringent fake upper limit is then searched for true coincidences. In this way, setting a significance of 0.999 on the null hypothesis test for each single trial, we achieve a global confidence of $\sim 99\%$, i.e. a false claim probability of $\sim 1\%$.

6. Results

As a last step, we searched for coincidences at the true time in all the selected configurations. The final outcome was consistent with no rejection of the null hypothesis test at 99.9% confidence for each configuration, corresponding to a global false claim probability of 1%. The confidence interval are, hence, upper limits on the rate of incoming GWs.

Detailed results are presented in table 2, where, for each injected waveform, the estimated efficiency, the average background, the zero-lag coincidence counts and the corresponding 95% upper limit are reported. Rescaling the listed efficiencies by their asymptotical values, we can easily infer that, for the 11 injected waveforms, the so-

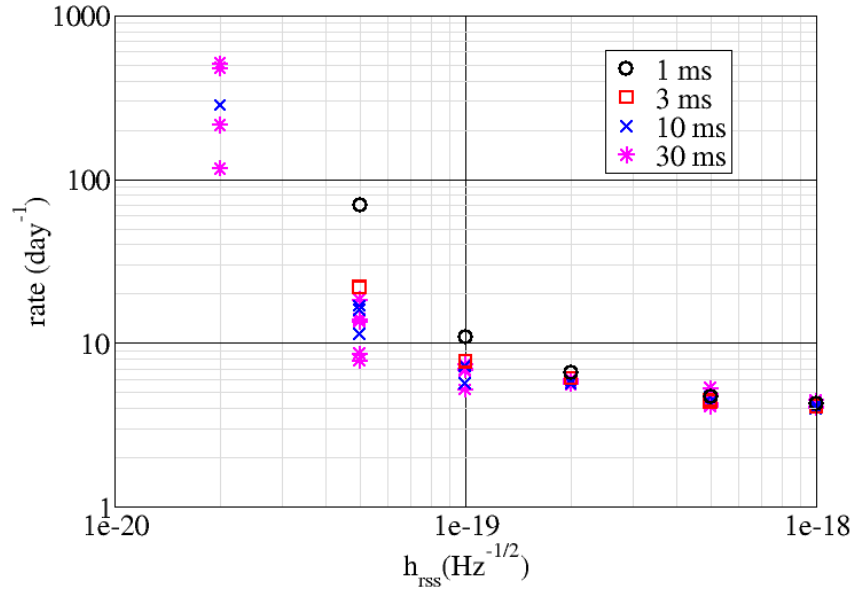


Figure 8. Upper limit at 95% conservative coverage on the event rate as a function of the population amplitude. Upper limits referring to the same duration of the signal but different central frequencies are grouped with the same symbol. Notice that the systematic error of about 10-30% on the amplitude calibration has not been taken into account.

called $h_{rss}^{50\%}$ || ranges from $5 \cdot 10^{-20}$ Hz $^{-1/2}$ (for the DS with central frequency $f_0=930$ Hz and $\tau=30$ ms for the AURIGA-NAUTILUS pair) to $1 \cdot 10^{-19}$ Hz $^{-1/2}$ (for the DS with central frequency $f_0=914$ Hz and $\tau=1$ ms for the AURIGA-Virgo pair). We included also a few configurations with low amplitude signals: in order to preserve the residual efficiencies, the related average backgrounds are quite high, leading to non null zero-delay coincidence counts.

Figure 8 shows the upper limits as a function of signal amplitude. The asymptote for large amplitude signals is inversely proportional to the observation time and to the asymptotical efficiency and depends on the confidence belt: for this 24 hr search, it is $\simeq 4.0$ events/day, as our maximum efficiency is $\simeq 90\%$ and the chosen confidence belt (see sec.5.3) with 95% C.L. sets a pretty conservative value (3.6 counts).

|| The signal amplitude with 50% detection probability.

Table 2: Results of the two-fold coincidence searches, for the chosen couples of detectors (see sec.5.4) and for each set of the waveform parameters and amplitudes (Second, third and fourth column). The last four columns represent, respectively, the efficiency of detection measured by means of MDC injections, the average accidental coincidence counts (N_b), the number of coincidences found at zero-delay (N_c) and the corresponding 95% upper limit. The errors associated with the efficiency and background estimates show the 1σ statistic fluctuation (*apices*).

detector pair	f_0 (Hz)	τ (ms)	h_{rss} ($\text{Hz}^{-1/2}$)	efficiency (%)	N_b	N_c	UL
AUR-VIR	914	1	$5 \cdot 10^{-20}$	$5.1^{\pm 0.3}$	$0.046^{\pm 0.011}$	0	69.2
AUR-VIR	914	1	$1 \cdot 10^{-19}$	$32.6^{\pm 0.7}$	$0.093^{\pm 0.016}$	0	10.9
AUR-VIR	914	1	$2 \cdot 10^{-19}$	$54.0^{\pm 0.8}$	$0.101^{\pm 0.016}$	0	6.6
AUR-NAU	914	1	$5 \cdot 10^{-19}$	$75.2^{\pm 0.7}$	$0.068^{\pm 0.014}$	0	4.7
AUR-NAU	914	1	$1 \cdot 10^{-18}$	$83.0^{\pm 0.6}$	$0.071^{\pm 0.014}$	0	4.3
AUR-VIR	914	1	$2 \cdot 10^{-18}$	$68.1^{\pm 0.7}$	$0.103^{\pm 0.017}$	0	5.2
AUR-VIR	882	3	$5 \cdot 10^{-20}$	$16.3^{\pm 0.6}$	$0.086^{\pm 0.015}$	0	21.9
AUR-VIR	882	3	$1 \cdot 10^{-19}$	$45.3^{\pm 0.8}$	$0.091^{\pm 0.016}$	0	7.8
AUR-VIR	882	3	$2 \cdot 10^{-19}$	$58.5^{\pm 0.8}$	$0.098^{\pm 0.016}$	0	6.1
AUR-EXP	882	3	$5 \cdot 10^{-19}$	$79.8^{\pm 0.6}$	$0.058^{\pm 0.012}$	0	4.5
AUR-EXP	882	3	$1 \cdot 10^{-18}$	$86.6^{\pm 0.5}$	$0.056^{\pm 0.012}$	0	4.1
AUR-VIR	882	3	$2 \cdot 10^{-18}$	$68.6^{\pm 0.7}$	$0.103^{\pm 0.017}$	0	5.2
AUR-VIR	946	3	$5 \cdot 10^{-20}$	$16.2^{\pm 0.6}$	$0.091^{\pm 0.016}$	0	22.0
AUR-VIR	946	3	$1 \cdot 10^{-19}$	$46.2^{\pm 0.8}$	$0.086^{\pm 0.015}$	0	7.7
AUR-VIR	946	3	$2 \cdot 10^{-19}$	$58.6^{\pm 0.8}$	$0.088^{\pm 0.015}$	0	6.1
AUR-NAU	946	3	$5 \cdot 10^{-19}$	$81.1^{\pm 0.6}$	$0.098^{\pm 0.016}$	0	4.4
EXP-NAU	946	3	$1 \cdot 10^{-18}$	$85.9^{\pm 0.5}$	$0.036^{\pm 0.010}$	0	4.1
AUR-VIR	946	3	$2 \cdot 10^{-18}$	$67.8^{\pm 0.7}$	$0.101^{\pm 0.016}$	0	5.2
AUR-VIR	866	10	$5 \cdot 10^{-20}$	$21.0^{\pm 0.6}$	$0.078^{\pm 0.014}$	0	16.9
AUR-VIR	866	10	$1 \cdot 10^{-19}$	$48.5^{\pm 0.8}$	$0.073^{\pm 0.014}$	0	7.3
AUR-VIR	866	10	$2 \cdot 10^{-19}$	$60.2^{\pm 0.7}$	$0.063^{\pm 0.013}$	0	5.9
AUR-EXP	866	10	$5 \cdot 10^{-19}$	$76.2^{\pm 0.6}$	$0.071^{\pm 0.014}$	0	4.7
AUR-EXP	866	10	$1 \cdot 10^{-18}$	$84.3^{\pm 0.6}$	$0.053^{\pm 0.012}$	0	4.2
AUR-VIR	866	10	$2 \cdot 10^{-18}$	$69.2^{\pm 0.7}$	$0.103^{\pm 0.017}$	0	5.1
AUR-VIR	898	10	$5 \cdot 10^{-20}$	$22.3^{\pm 0.6}$	$0.083^{\pm 0.015}$	0	15.9
AUR-VIR	898	10	$1 \cdot 10^{-19}$	$49.4^{\pm 0.8}$	$0.088^{\pm 0.015}$	0	7.2
AUR-VIR	898	10	$2 \cdot 10^{-19}$	$60.4^{\pm 0.7}$	$0.088^{\pm 0.015}$	0	5.9

continue ...

Table 2 continued

detector pair	f_0 (Hz)	τ (ms)	h_{rss} ($\text{Hz}^{-1/2}$)	efficiency (%)	N_b	N_c	UL
AUR-EXP	898	10	$5 \cdot 10^{-19}$	$82.8^{\pm 0.6}$	$0.066^{\pm 0.013}$	0	4.3
AUR-EXP	898	10	$1 \cdot 10^{-18}$	$87.7^{\pm 0.5}$	$0.068^{\pm 0.014}$	0	4.1
AUR-VIR	898	10	$2 \cdot 10^{-18}$	$69.2^{\pm 0.7}$	$0.098^{\pm 0.016}$	0	5.1
AUR-VIR	930	10	$2 \cdot 10^{-20}$	$2.4^{\pm 0.2}$	$4.1^{\pm 0.10}$	4	283.9
AUR-VIR	930	10	$5 \cdot 10^{-20}$	$31.1^{\pm 0.7}$	$0.071^{\pm 0.014}$	0	11.4
AUR-NAU	930	10	$1 \cdot 10^{-19}$	$61.9^{\pm 0.7}$	$0.068^{\pm 0.014}$	0	5.7
AUR-VIR	930	10	$2 \cdot 10^{-19}$	$62.7^{\pm 0.7}$	$0.081^{\pm 0.015}$	0	5.7
EXP-NAU	930	10	$5 \cdot 10^{-19}$	$83.7^{\pm 0.6}$	$0.036^{\pm 0.010}$	0	4.3
AUR-NAU	930	10	$1 \cdot 10^{-18}$	$89.4^{\pm 0.5}$	$0.083^{\pm 0.015}$	0	4.0
AUR-VIR	930	10	$2 \cdot 10^{-18}$	$69.3^{\pm 0.7}$	$0.103^{\pm 0.017}$	0	5.1
AUR-VIR	866	30	$2 \cdot 10^{-20}$	$2.1^{\pm 0.2}$	$9.1^{\pm 0.15}$	11	508.1
AUR-VIR	866	30	$5 \cdot 10^{-20}$	$25.5^{\pm 0.7}$	$0.021^{\pm 0.007}$	0	14.0
AUR-VIR	866	30	$1 \cdot 10^{-19}$	$51.9^{\pm 0.8}$	$0.013^{\pm 0.006}$	0	6.8
AUR-VIR	866	30	$2 \cdot 10^{-19}$	$61.8^{\pm 0.7}$	$0.053^{\pm 0.012}$	0	5.8
AUR-VIR	866	30	$5 \cdot 10^{-19}$	$66.5^{\pm 0.7}$	$0.051^{\pm 0.012}$	0	5.3
AUR-EXP	866	30	$1 \cdot 10^{-18}$	$78.8^{\pm 0.6}$	$0.068^{\pm 0.014}$	0	4.5
AUR-VIR	866	30	$2 \cdot 10^{-18}$	$69.2^{\pm 0.7}$	$0.111^{\pm 0.017}$	0	5.1
AUR-VIR	874	30	$2 \cdot 10^{-20}$	$2.4^{\pm 0.2}$	$9.5^{\pm 0.15}$	12	476.2
AUR-VIR	874	30	$5 \cdot 10^{-20}$	$26.4^{\pm 0.7}$	$0.046^{\pm 0.011}$	0	13.5
AUR-VIR	874	30	$1 \cdot 10^{-19}$	$51.5^{\pm 0.8}$	$0.033^{\pm 0.009}$	0	6.9
AUR-VIR	874	30	$2 \cdot 10^{-19}$	$61.6^{\pm 0.7}$	$0.043^{\pm 0.011}$	0	5.8
AUR-EXP	874	30	$5 \cdot 10^{-19}$	$73.1^{\pm 0.7}$	$0.076^{\pm 0.014}$	0	4.9
AUR-EXP	874	30	$1 \cdot 10^{-18}$	$82.3^{\pm 0.6}$	$0.063^{\pm 0.013}$	0	4.3
AUR-VIR	874	30	$2 \cdot 10^{-18}$	$69.8^{\pm 0.7}$	$0.111^{\pm 0.017}$	0	5.1
AUR-VIR	906	30	$5 \cdot 10^{-20}$	$19.4^{\pm 0.6}$	$0.086^{\pm 0.015}$	0	18.4
AUR-EXP	906	30	$1 \cdot 10^{-19}$	$48.0^{\pm 0.8}$	$0.061^{\pm 0.013}$	0	7.4
AUR-VIR	906	30	$2 \cdot 10^{-19}$	$59.5^{\pm 0.7}$	$0.068^{\pm 0.014}$	0	6.0
AUR-EXP	906	30	$5 \cdot 10^{-19}$	$82.8^{\pm 0.6}$	$0.066^{\pm 0.013}$	0	4.3
AUR-EXP	906	30	$1 \cdot 10^{-18}$	$86.3^{\pm 0.5}$	$0.066^{\pm 0.013}$	0	4.1
AUR-VIR	906	30	$2 \cdot 10^{-18}$	$69.3^{\pm 0.7}$	$0.103^{\pm 0.017}$	0	5.1
AUR-VIR	930	30	$2 \cdot 10^{-20}$	$9.3^{\pm 0.4}$	$16.3^{\pm 0.20}$	16	116.2
AUR-NAU	930	30	$5 \cdot 10^{-20}$	$45.4^{\pm 0.8}$	$0.043^{\pm 0.011}$	0	7.8
AUR-NAU	930	30	$1 \cdot 10^{-19}$	$69.0^{\pm 0.7}$	$0.056^{\pm 0.012}$	0	5.2
AUR-VIR	930	30	$2 \cdot 10^{-19}$	$64.0^{\pm 0.7}$	$0.023^{\pm 0.008}$	0	5.6
EXP-NAU	930	30	$5 \cdot 10^{-19}$	$85.5^{\pm 0.5}$	$0.028^{\pm 0.009}$	0	4.2
AUR-NAU	930	30	$1 \cdot 10^{-18}$	$90.0^{\pm 0.5}$	$0.081^{\pm 0.015}$	0	4.0
AUR-VIR	930	30	$2 \cdot 10^{-18}$	$69.6^{\pm 0.7}$	$0.106^{\pm 0.017}$	0	5.1
AUR-NAU	938	30	$2 \cdot 10^{-20}$	$4.6^{\pm 0.3}$	$3.0^{\pm 0.09}$	6	214.1
AUR-NAU	938	30	$5 \cdot 10^{-20}$	$41.3^{\pm 0.7}$	$0.068^{\pm 0.014}$	0	8.6

continue ...

Table 2 continued

detector pair	f_0 (Hz)	τ (ms)	h_{rss} ($\text{Hz}^{-1/2}$)	efficiency (%)	N_b	N_c	UL
AUR-NAU	938	30	$1 \cdot 10^{-19}$	$68.1^{\pm 0.7}$	$0.078^{\pm 0.014}$	0	5.2
AUR-VIR	938	30	$2 \cdot 10^{-19}$	$63.0^{\pm 0.7}$	$0.056^{\pm 0.012}$	0	5.6
AUR-NAU	938	30	$5 \cdot 10^{-19}$	$86.9^{\pm 0.5}$	$0.081^{\pm 0.015}$	0	4.1
AUR-EXP	938	30	$1 \cdot 10^{-18}$	$86.3^{\pm 0.5}$	$0.073^{\pm 0.014}$	0	4.1
AUR-VIR	938	30	$2 \cdot 10^{-18}$	$70.2^{\pm 0.7}$	$0.098^{\pm 0.016}$	0	5.1

7. Final remarks

We presented a methodological study for analyzing data collected by a network of non-homogeneous detectors. The search was aimed at detecting transient GW signals. We implemented a two-fold time coincidence search; however, this method could be applied as well to any detectors combination, e.g. three-fold, logical “OR” of two-fold, etc.. For each set of waveform parameters and amplitude, 6 different couples of detectors were available: we chose to perform our search on those couples which allow potentially the set up of the most stringent upper limit (see sect. 5.4).

The key point of the method is the optimization process of the analysis thresholds for a given source population by means of Monte Carlo MDC injections.

Although the proposed methodology is viable for any specific signal model, including the sky distribution of the sources, in the preset study we assumed DS signals incoming from the GC, limiting our observation range to our galaxy.

Moreover, in order to estimate the detection efficiency of the network we applied a standard Monte Carlo procedure based on a large set of injected signals. Although this software technique is computational intensive, it permits to derive reliable values of the efficiency and unbiased physical interpretation of the results, i.e. the GW amplitudes and rates of the population under study.

Finally we notice that in the procedure presented here, the statistical test relies just on the event magnitude. However, we stress that it is possible to extend the method either by including other statistical tests in the definition of the local Event Trigger Generators or by implementing a common maximum likelihood estimator (χ^2 test).

8. Acknowledgments

We acknowledge the funding from EU FP6 programme - ILIAS. Lucio Baggio was supported by the EGO Consortium. Virginia Re was supported by EGO-VESF fellowship, call 2005.

Appendix A. Optimization pipeline

We present here a schematic overview of all the steps:

- A specific search algorithm for each detector is run in order to produce lists of triggers. For each trigger the time and an estimate of the SNR ratio are exchanged. The exchanged lists comprise one derived by the analysis of the plain data from the detector, and others obtained by adding to the data different MDC channels before running the event search algorithm.

Coincidence search

- For each couple of detectors, the plain data sets are searched for coincidences after adding 800 offsets in steps of 1s, with a time window of 40ms. This covers about 7 minutes before and after the unshifted time, with a safety range of $\pm 20s$ around the zero-delay time¶.
- All the lists with MDC injections are searched for coincident events (obviously no time delay analysis is performed in these cases) and the detection efficiency is thus evaluated.

Optimization procedure

- The data are split into two equal sets, one used in the optimization phase, the other in the estimation phase, by alternating shift index.
- The data are divided in 30 minutes long time bins .
- We evolve a couple of staircase thresholds (jointly for the two detectors) by increasing the threshold level in one time bin and one detector at a time. At each step, in order to have a significant variation, the test threshold is increased by an amount which corresponds to a reduction in the background counts of the order of the standard deviation of the counts themselves⁺.
- At the n th step of the algorithm, we compute the ratio $N_{eff}^{(n)} / \sqrt{N_b^{(n)}}$, where $N_{eff}^{(n)}$ and $N_b^{(n)}$ are the *total* number of MDC coincidences and background coincidences from the set reserved for the optimization whose associated amplitudes are above the n th set of thresholds. Then the effect of increasing the threshold of one level at one bin is evaluated by computing the new ratio $N_{eff}^{(n+1)} / \sqrt{N_b^{(n+1)}}$. Every time the bins in both detectors are tried one by one in order to find for which a threshold change would score the higher benchmark. If this benchmark is better than the one obtained at the previous step, the level for that bin is changed, and this is taken as the starting point for the next loop. Instead, if all changes resulted in a decrease of

¶ We recall that 10s is the maximum value for the blind shift applied previously to data exchange, see section 3.

⁺ We found empirically that the square root of the counts divided by 6 is a good compromise. Yet, we impose that the background decrease of at least 4 counts.

the benchmark, the loop is exited. The loop will otherwise continue up to reaching the higher level of thresholds.

- When a time bin is found contributing to the efficiency by less than 0.1% the threshold in that bin is raised until no background event is surviving. Similarly to what was done, at the end of the previous loop we recompute the benchmark $N_{eff}/\sqrt{N_b}$ to see whether removing the bin would be an improvement. These actions mitigate the possibility that the algorithm converges to a false maximum with relatively high background.
- The found set of thresholds are applied to the alternative sets of triggers which were kept aside in order to re-estimate unbiased values for N_{eff} and N_b . These two numbers, divided respectively by the number of injected events (4320) and of time-shifted configurations (400), give the estimates for the efficiency of detection and for the average background counts.

Efficiency and confidence

- For each shifted configuration of the alternative set, the number of coincident events is used to compute the corresponding upper limit at 95% confidence.
- This entire procedure is repeated for a different couple of detectors and/or a different set of MDC injections.
- After having decided the level of confidence for the eventual rejection of the Null hypothesis, we unveil the coincidence counts at zero-delay, and compute for them the confidence interval.

Appendix B. Details about the injected signals

In this study we assume that the waveforms, in the TT gauge are of the form

$$\begin{aligned}
 \begin{pmatrix} h_+ \\ h_\times \end{pmatrix} &= \frac{h_{rss}}{\pi f_{gw} \tau} \sqrt{\frac{1 + 4\pi^2 f_{gw}^2 \tau^2}{\tau (1 + e^{-1/(2f_{gw}\tau)})}} e^{-t/\tau} \\
 &\times \begin{pmatrix} \cos 2\psi & -\sin 2\psi \\ \sin 2\psi & \cos 2\psi \end{pmatrix} \\
 &\times \begin{pmatrix} \frac{1+\cos^2 \iota}{2} & \Theta(t - \frac{1}{4f_{gw}}) \cos(2\pi f_{gw} t) \\ \cos \iota & \Theta(t) \sin(2\pi f_{gw} t) \end{pmatrix} \tag{B.1}
 \end{aligned}$$

where the angle ψ is an arbitrary polarization and the angle ι an arbitrary inclination of the angular momentum of the system which originates the burst with respect to the line of sight.

Notice the different Θ for the h_+ and h_\times terms; the reason for multiplying $\cos(2\pi f_{gw}t)$ by $\Theta\left(1 - \frac{1}{4f_{gw}}\right)$ is to avoid a discontinuity at the beginning of the waveform, which would result into an infinite energy, even though h_{rss} would remain finite.

The polarization ψ is uniformly distributed in $[0, 2\pi)$, while $\cos i$ is uniformly distributed in $[-1, 1)$; these choices correspond to assume a random orientation in space of the axis of symmetry of the emitting system.

Appendix B.1. Signal normalization

The signal normalization is done requiring equation (B.2) for $\psi = 0, \iota = 0$:

$$h_{rss}^2 \equiv \int_0^\infty (|h_+(t)|^2 + |h_\times(t)|^2) dt. \quad (\text{B.2})$$

It can also be useful to relate h_{rss} and the energy emitted E assuming a source located at a distance r . To this end, we recall the standard definition of the energy flux

$$\frac{dE}{dAdf} = \frac{\pi c^3}{2G_N} f^2 \left(|\tilde{h}_+(f)|^2 + |\tilde{h}_\times(f)|^2 \right) \quad (\text{B.3})$$

where $dA = r^2 d\Omega$. It is straightforward to compute

$$\begin{aligned} \left(|\tilde{h}_+(f)|^2 + |\tilde{h}_\times(f)|^2 \right) &= h_{rss}^2 \frac{\tau \left(4f_{gw}^2 \pi^2 \tau^2 + 1 \right)}{\left(1 + e^{\frac{1}{2f_{gw}\tau}} \right)} \\ &\times \frac{\left(\cos^4(i) + \left(2 + 4e^{\frac{1}{2f_{gw}\tau}} \right) \cos^2(i) + 1 \right)}{\left(16f^4 \pi^4 \tau^4 + \left(4f_{gw}^2 \pi^2 \tau^2 + 1 \right)^2 + f^2 \left(8\pi^2 \tau^2 - 32f_{gw}^2 \pi^4 \tau^4 \right) \right)} \end{aligned} \quad (\text{B.4})$$

and then, after performing the integral over frequencies and the angles, one obtains:

$$E = \frac{\pi c^3 r^2 h_{rss}^2 \left(4f_{gw}^2 \pi^2 \tau^2 + 1 \right)}{2G_N} \frac{\left(7 + 5e^{\frac{1}{2f_{gw}\tau}} \right)}{30 \left(1 + e^{\frac{1}{2f_{gw}\tau}} \right) \pi \tau^2} \quad (\text{B.5})$$

i.e.:

$$\begin{aligned} \frac{E}{M_\odot c^2} &\simeq 10^{-6} \frac{\left(1 + (5/7)e^{\frac{1}{2f_{gw}\tau}} \right)}{\left(1 + e^{\frac{1}{2f_{gw}\tau}} \right)} \left(1 + \frac{1}{4\pi^2 \tau^2 f_{gw}^2} \right) \\ &\times \left[\frac{h_{rss}}{10^{-21}/\sqrt{Hz}} \right]^2 \left[\frac{r}{10 \text{ kpc}} \right]^2 \left[\frac{f_{gw}}{1 \text{ kHz}} \right]^2 \end{aligned} \quad (\text{B.6})$$

which means that observing an $h_{rss} \simeq 10^{-21}/\sqrt{Hz}$ with signals at about 1kHz corresponds to a source emitting a fraction $\sim 10^{-6}$ of a solar mass in gravitational waves at a distance of 10kpc.

References

- [1] Baggio L *et al* 2005 *Phys. Rev. Lett.* **94** 241101
- [2] Vinante A (for the AURIGA Collaboration) 2006 *Class. Quantum Grav.* **23** S103
- [3] Astone P (for the ROG Collaboration) 2004 *Class. Quantum Grav.* **21** (<http://stacks.iop.org/0264-9381/21/S1585>)
- [4] Astone P, *et al* 2006 *Class. Quantum Grav.* **23** S57 (<http://stacks.iop.org/0264-9381/23/S57>)
- [5] Acernese F (for the Virgo collaboration) 2006 *Class. Quantum Grav.* **23** S635 and referencies therein
- [6] Allen B Z (for the IGEC Collaboration) 2000 *Phys. Rev. Lett.* **85** 5046
- [7] Astone P *et al* (IGEC Collaboration) 2003 *Phys. Rev. D* **68** 022001
- [8] Astone P *et al* 2002 *Class. Quantum Grav.* **19** 5449
- [9] Abbott B *et al* (LIGO Scientific Collaboration) 2004 *Phys. Rev. D* **69** 102001
- [10] Abbott B *et al* (LIGO Scientific Collaboration) 2005 *Phys. Rev. D* **72** 062001
- [11] Abbott B *et al* (LIGO Scientific Collaboration) 2006 *Class. Quantum Grav.* **23** S653
- [12] Abbott B *et al* (LIGO Scientific Collaboration) 2005 *Phys. Rev. D* **72** 122004
- [13] Cadonati L *et al* 2005 *Class. Quantum Grav.* **22** S1337
- [14] Poggi S, Salemi F (for the AURIGA collaboration) and Cadonati L (for the LIGO Scientific collaboration) 2006 *J. Phys.: Conf. Ser.* **32** 198
- [15] Kokkotas K D and Schmidt B G 1999 <http://www.livingreviews.org/lrr-1999-2>
- [16] Ferrari V *et al* 2003 *Mon. Not. Roy. Astron. Soc.* **342** 629
- [17] Guidi G M, Cuoco E and Viceré A 2004 *Class. Quantum Grav.* **21** S815
- [18] S. Klimenko *et al* LIGO-T050222-00-Z
- [19] Astone P *et al.* 1997 *Il Nuovo Cimento* **20**
- [20] D'Antonio S 2002 *Class. Quantum Grav.* **19** 1499
- [21] Caron B, Flaminio R, Marion F, Mours B, Verkindt D, Cavalier F and Viceré A 1999 *Astrop. Phys.* **10** 369
- [22] Drago M, private communication
- [23] Astone P, D'Antonio S and Pai A 2006 *J. Phys.: Conf. Ser.* **32** 192
- [24] Feldman G J and Cousins R D 1998 *Phys. Rev. D* **57** 3873
- [25] Baggio L and Prodi G A 2003 *Statistical problems in particle physics, astrophysics and cosmology* ed R Mount, L Lyons and R Reitmeyer (Stanford) 238 (<http://www.slac.stanford.edu/econf/C030908/papers/WELT003.pdf>, arXiv:astro-ph/0312353)